

Simulations of Interacting Binary Systems - Pathways to Radio Bright GRB Progenitors

ANGEL HERNANDEZ ^{1, 2, *} ROSEANNE M. CHENG ^{3, 2, 4} NICOLE LLOYD-RONNING ^{2, 5, 6} AND C. E. FIELDS ^{5, 2, 7, †}

¹*Department of Physics, University of Colorado at Boulder; Boulder, CO 80309-0390, USA*

²*CCS-2, Computational Physics and Methods, Los Alamos National Laboratory, Los Alamos, NM 87544, USA*

³*T-3, Fluid Dynamics and Solid Mechanics, Los Alamos National Laboratory, Los Alamos, NM 87544, USA*

⁴*Department of Physics and Astronomy, University of New Mexico, Albuquerque, NM 87106, USA*

⁵*Center for Theoretical Astrophysics, Los Alamos National Laboratory, Los Alamos, NM 87544, USA*

⁶*Department of Math, Science and Engineering, University of New Mexico, Los Alamos, NM 87544, USA*

⁷*Steward Observatory, University of Arizona, Tucson, AZ 85721, USA*

ABSTRACT

Although the association of gamma-ray bursts (GRBs) with massive stellar death is on firm footing, the nature of the progenitor system and the key ingredients required for a massive star to produce a gamma-ray burst remain open questions. Here, we investigate the evolution of a massive star with a closely orbiting compact object companion using the stellar evolution code MESA. In particular, we examine how the companion influences the angular momentum and circumstellar environment near the end of the massive star life. We find that tidal effects can cause the compact object companion to significantly increase the angular momentum of the massive star, for orbital periods in the range of up to ~ 4 days. We model the density profile evolution of the massive star and discuss how tidal interactions may also lead to stripping of the outer stellar envelope in a way that can create an environment around the binary system that deviates from a typical $1/r^2$ wind density profile. We show how our results depend on the metallicity of the system, initial spin of the star, mass ratio, as well as accretion and dynamo prescriptions in the simulations. We conclude that these systems may be viable progenitors for radio-bright, long gamma-ray bursts.

Keywords: Gamma-ray bursts — Black Holes — Interacting Binaries

1. INTRODUCTION

Gamma-ray bursts (GRBs) are the most luminous objects in the universe. The connection between so-called long GRBs (LGRBs; those with prompt gamma-ray emission lasting more than two seconds) and the deaths of massive stars is strongly supported, both theoretically and observationally, including the direct association of supernova events with many LGRBs (Woosley 1993; MacFadyen & Woosley 1999; Bloom et al. 2002; Hjorth et al. 2003; Woosley & Bloom 2006; Woosley & Heger 2006; Kumar et al. 2008a,b; Hjorth & Bloom 2012; Lyman et al. 2017). While stars with high angular momentum and a stripped hydrogen envelope are necessary

ingredients, the exact conditions required to produce an LGRB from a collapsing star (MacFadyen & Woosley 1999; Yoon & Langer 2005; Hirschi et al. 2005; Yoon et al. 2006; Woosley & Heger 2006), and indeed the jet launching mechanism itself (e.g. Barkov & Komissarov 2008; Komissarov & Barkov 2009; Lloyd-Ronning et al. 2019a; King & Pringle 2021), remain uncertain. It is an ongoing pursuit to determine and understand *which* stars make gamma-ray bursts, and *why*.

This mystery has been further deepened by the recent evidence (Lloyd-Ronning & Fryer 2017; Lloyd-Ronning et al. 2019b; Chakraborty et al. 2023) that those GRBs with radio afterglows (so-called radio-bright GRBs) appear to have significantly *longer-lasting prompt gamma-ray duration* and higher isotropic equivalent energy than their radio-dark counterparts. It has been suggested (Lloyd-Ronning 2022) that these radio bright GRBs may be a result of a massive star collapsing in a system with an influential compact object companion. Under the right conditions, the companion can spin up

Corresponding author:
angel.hernandez@colorado.edu

* McNair Scholar, Science Undergraduate Laboratory Internships (SULI) Fellow

† Feynman Distinguished Postdoctoral Fellow

the massive star, providing it the angular momentum it needs to create a longer lasting jet and therefore longer-lasting prompt gamma-ray burst; this companion may also cause a more extended and dense circumburst environment, providing the surrounding gas needed for the GRB to shine brightly in the radio band.

In this paper, we test the hypothesis that long duration, radio-bright GRBs could result from a massive star collapsing in an interacting binary system with a closely orbiting compact object companion. In particular, we explore the influence of a black hole companion over a range of phase space varying orbital period, metallicity, initial spin of the star, mass ratio, accretion rate, magnetic fields, and numerical stopping conditions. We use the well-developed, open-source stellar evolution code *Modules for Experiments in Stellar Astrophysics* (MESA) to perform this study. We present the parameter space in which this system will produce a highly-spinning massive star with a potentially dense extended circumburst environment - exactly the conditions needed to produce a radio-bright GRB.

Our paper is organized as follows: In §2, we describe the code and simulation set-up (with a convergence study discussed in our Appendix). In §3, we present our results and show the range of initial conditions that lead to a substantial spin up of the massive star in our systems. Additionally, we provide representative density profiles of the massive star and discuss the implications for the density profile of the circumbinary medium. In §4, we present discussion and caveats to our results. In §5, we summarize our main conclusions and discuss future work to support this effort.

2. CODE AND SIMULATION SET-UP

We use the one-dimensional stellar evolution code *Modules for Experiments in Stellar Astrophysics* (MESA) for our simulations (Paxton et al. 2011, 2013, 2015, 2018, 2019; Paxton 2021; Jermyn et al. 2023)¹. MESA solves the coupled structure and composition equations simultaneously. The MESA equation of state (EOS) is a blend of the OPAL (Rogers & Nayfonov 2002), SCVH (Saumon et al. 1995), FreeEOS (Irwin 2004), HELM (Timmes & Swesty 2000), PC (Potekhin & Chabrier 2010), and Skye (Jermyn et al. 2021b) EOSes. Radiative opacities are primarily from OPAL (Iglesias & Rogers 1993, 1996), with low-temperature data from Ferguson et al. (2005) and the high-temperature, and the Compton-scattering dominated regime by Poutanen (2017). Electron conduction opacities are from Casisi et al. (2007) and Blouin et al. (2020). Nuclear re-

action rates are from JINA REACLIB (Cyburt et al. 2010), NACRE (Angulo et al. 1999) and additional tabulated weak reaction rates Fuller et al. (1985); Oda et al. (1994); Langanke & Martínez-Pinedo (2000). Screening is included via the prescription of Chugunov et al. (2007). Thermal neutrino loss rates are from Itoh et al. (1996). Roche lobe radii in binary systems are computed using the fit of Eggleton (1983). Mass transfer rates in Roche lobe overflowing binary systems are determined following the prescription of Ritter (1988).

We employ the binary module in MESA because it enables simultaneous evolution of an interacting pair of stars undergoing transfer of mass and angular momentum (Paxton et al. 2015). We use the stellar rotation and tidal interaction treatment for the binary evolution from Marchant (2019) and Mink (2019). With these tools, we investigate the tidal regime where a black hole (BH) companion significantly influences the evolution of a massive star prior to collapse. Again, we are in particular searching for the parameter space for which the companion can spin up the massive star, and also produce tidal effects that may lead to a denser (relative to a single massive star), extended circumbinary medium into which the GRB jet will travel. We describe the details of our simulation set-up below.

2.1. MESA Input Physics

We evolve a Zero Aged Main Sequence (ZAMS) star with a point mass companion at different mass ratios, orbital periods², metallicities, stellar rotations, and mass/angular momentum transfer schemes. Table 1 gives the choice of parameters for our simulations. A short description of our initial set-up is as follows:

- Mass ratio - We consider a $25 M_{\odot}$ massive star with either a $10 M_{\odot}$ or $15 M_{\odot}$ BH companion as physically viable systems, created in situ or by dynamical capture. Systems with these mass ratios have been observed in X-ray binaries (Kelley et al. 1983; Levine et al. 1993, 2000; Tauris & van den Heuvel 2006; Falanga et al. 2015). In future work, we perform population synthesis models (see, e.g., Cason et al. 2024) to place constraints on the numbers of these systems we expect in our universe. However, for now, we assume these systems exist in sufficient numbers and focus on their individual evolution.

¹ We use MESA release r21.12.1.

² We consider orbital periods of the BH that lead to significant tidal interaction but do not consider common envelope or merger scenarios.

Table 1. Massive star and black hole binary simulation parameters that lead to high angular momentum progenitor systems for radio bright IGRB. We give the model name, stellar mass M_* in solar mass units M_\odot , black hole mass M_{BH} in solar mass units M_\odot , orbital period τ in days, metallicity Z , initial orbital separation of the binary $a_{orb,i}$ in solar radius units R_\odot , initial total angular momentum of the binary $J_{tot,i}$ in CGS units, and final stellar spin up angular momentum of the star ΔJ_{spin} in CGS units. The stellar radius for a $25 M_\odot$ star is $R_* = \{4.445, 6.058\} R_\odot$ for $Z = \{10^{-4}, 10^{-2}\}$. For all simulations listed, we consider an initially non-rotating massive star. Additionally, we consider initial rotations or stellar spin velocities at $v_1 = 9.177 \times 10^1$ km/s and $v_* = \{5.199 \times 10^2, 4.450 \times 10^2\}$ km/s for $Z = \{10^{-4}, 10^{-2}\}$ stellar models at a star-to-black-hole mass ratio of $25M_\odot$ and $15M_\odot$ with a 3-day orbital period.

Model name	$M_* [M_\odot]$	$M_{BH} [M_\odot]$	τ [days]	Z	$a_{orb,i} [R_\odot]$	$J_{tot,i} [\text{g cm}^{-2} \text{ s}^{-1}]$	$\Delta J_{spin} [\text{g cm}^{-2} \text{ s}^{-1}]$
MS25_BH15_T1.5_Z1.0e-4	25	15	1.5	10^{-4}	18.86	1.556×10^{54}	4.144×10^{52}
MS25_BH15_T2.0_Z1.0e-4	25	15	2.0	10^{-4}	22.85	1.712×10^{54}	3.857×10^{52}
MS25_BH15_T2.5_Z1.0e-4	25	15	2.5	10^{-4}	26.51	1.845×10^{54}	3.398×10^{52}
MS25_BH15_T3.0_Z1.0e-4	25	15	3.0	10^{-4}	29.94	1.960×10^{54}	2.864×10^{52}
MS25_BH15_T4.0_Z1.0e-4	25	15	4.0	10^{-4}	36.27	2.157×10^{54}	2.000×10^{52}
MS25_BH15_T1.5_Z1.0e-2	25	15	1.5	10^{-2}	18.86	1.556×10^{54}	4.948×10^{52}
MS25_BH15_T2.0_Z1.0e-2	25	15	2.0	10^{-2}	22.85	1.712×10^{54}	4.267×10^{52}
MS25_BH15_T2.5_Z1.0e-2	25	15	2.5	10^{-2}	26.51	1.845×10^{54}	3.863×10^{52}
MS25_BH15_T3.0_Z1.0e-2	25	15	3.0	10^{-2}	29.94	1.960×10^{54}	3.598×10^{52}
MS25_BH15_T4.0_Z1.0e-2	25	15	4.0	10^{-2}	36.27	2.157×10^{54}	3.236×10^{52}
MS25_BH10_T1.5_Z1.0e-4	25	10	1.5	10^{-4}	18.04	1.084×10^{54}	4.347×10^{52}
MS25_BH10_T3.0_Z1.0e-4	25	10	3.0	10^{-4}	28.63	1.366×10^{54}	2.811×10^{52}
MS25_BH10_T1.5_Z1.0e-2	25	10	1.5	10^{-2}	18.04	1.084×10^{54}	5.214×10^{52}
MS25_BH10_T3.0_Z1.0e-2	25	10	3.0	10^{-2}	28.63	1.366×10^{54}	3.755×10^{52}

- **Orbital Period** - We consider orbital periods (and subsequently orbital separations) where the BH companion may tidally influence the massive star at a distance beyond the star’s radius outside of the Roche lobe radius of the massive star. Furthermore, at these separations, a Newtonian treatment to the gravitational interaction of the binary is sufficient because the general relativistic corrections to the orbit and tide are very small.
- **Metallicity** - We consider two values, $Z = 10^{-4}$ and $Z = 10^{-2}$, where metallicity Z is defined as the mass fraction elements heavier than helium relative to the total mass of the gas. We note that these span two orders of magnitude but remain lower than solar metallicity ($\sim 1.7 \times 10^{-2}$), while it has been demonstrated that long GRBs tend to occur on average in lower metallicity environments (Fruchter et al. 1999; Le Floch et al. 2003; Fruchter et al. 2006; Levesque et al. 2010; Graham & Fruchter 2013, 2017; Palla et al. 2019; Graham et al. 2019). Nonetheless, these values still provide the endpoints to a large dynamic range over which to explore dependencies on metallicity.
- **Spin Synchronization** - We use the stellar rotation (in binary systems) settings in Marchant (2019), who model systems similar to what we are considering here. In particular, we turn on a spin synchronization flag which enables the tidal spin up of a massive star by its companion. We keep the default of no initial relaxation of the stellar rotation to the orbital period.
- **Massive star initial rotation** - We consider a range of zero and non-zero initial rotations for the massive star. We initialize massive star non-zero rotation at a velocity given by the binary evolution equations in Hurley et al. (2000) and Hurley et al. (2002), used in the binary population synthesis code COSMIC Breivik et al. (2020). We take specific values from the COSMIC output discussed in Kenoly et al. (2023). Additionally, we consider higher velocity initial conditions for the massive star at half of the break-up velocity.
- **Mass transfer** - For the simulations in this paper, the BH companion is primarily beyond the Roche lobe of the massive star and outside the regime where the choice of mass transfer scheme between the massive star and its companion is important.

We employ the default setting for MESA (a Kolb-Ritter (Kolb & Ritter 1990) mass transfer scheme) and further constrain the mass transfer to be lower than the Eddington limit. We note that there are many subtleties that come into play when choosing the mass transfer prescriptions. For example, Cehula & Pejcha (2023) find an intermediate solution between optically thin and optically thick regimes for Roche lobe overflow; their model finds a mass transfer rate about two times smaller than Kolb & Ritter (1990) and four times smaller than Marchant (2019) for a $30 M_{\odot}$, low metallicity star. However, again, because we are considering encounters where the initial separation distances are larger than the Roche lobe radius, these subtleties generally do not influence our main results.

We set the prescription for angular momentum loss through mass transfer according to the results of de Mink et al. (2013); Mink (2019); Marchant (2019), who carefully examine how angular momentum is lost and/or transferred between stars in a binary system, for different evolutionary stages, chemical composition, masses, separations, and magnetic field configurations.

- Spruit-Taylor Dynamo - Through magnetic coupling between layers in the stellar interior, the Spruit-Taylor dynamo (Spruit 2002) is a possible pathway to transport angular momentum within the massive star, potentially leading to a spin down. However, as we discuss below, its effect is more pronounced in stars less massive than those we consider here. Nonetheless, we have run simulations with this flag both on and off and find a negligible impact on our results (we discuss this further below).
- Rotation in Convection Zone - In the case of rotation in the convection zone, angular momentum can be transported through various processes internal to the star (Augustson & Mathis 2019). These processes are controlled by the diffusion coefficients of Goldreich-Schubert-Fricke, Eddington-Sweet circulation, secular shear instability, and dynamical shear instability (see, e.g. Heger et al. 2000, for a description). We use the default MESA settings for rotation in the convection zone as well as the diffusion coefficients.

- Stopping Condition - We identify the end point for our simulations as the stage prior to collapse when the carbon-oxygen core forms at $\sim 6-8$ Myr with a corresponding rapid increase in central temperature and density within the star. We report the maximum angular momentum transfer to the star prior to this stage in the simulated evolution.

In the following, we present our set of binary parameters that lead to viable progenitors of radio bright LGRBs, particularly through significant stellar spin up over the massive star lifetime due to interaction with its companion. In our numerical simulations, we track the evolution of quantities that describe the dynamics of the binary system such as stellar and BH mass, orbital separation of the binary, and change in spin, orbital, and total angular momentum as well as stellar quantities through radial profiles in density and temperature. In the Appendix, we discuss convergence studies of representative models MS25_BH15_T3.0_Z1.0e-4 and MS25_BH15_T3.0_Z1.0e-2 of the tidal interaction. We show that these quantities do not change appreciably over stellar lifetime and model number at increasing mass resolution. Additionally, we identify the end point in our simulations prior to collapse in tracking the evolution of the spin up of the massive star with the formation of the carbon-oxygen core.

3. RESULTS

3.1. Spin up of the Massive Star

For the binary parameters given in Table 1, our numerical simulations show a significant spin up of the massive star due to the tidal interaction with a BH, consistent with analytic estimates for long GRB binary progenitors (Lloyd-Ronning 2022). In the following, we describe how these changes in spin angular momentum for the massive star depend on stellar metallicity, massive star to BH mass ratio, and initial stellar spin.

3.1.1. Dependence on Metallicity

In Fig. 1, we show the change in angular momentum of the massive star with initial orbital period and corresponding orbital separation for two stellar metallicities at $Z = 10^{-4}$ (left panels) and $Z = 10^{-2}$ (right panels). In the top row, we give the change in spin angular momentum ΔJ_{spin} or extent to which the star is spun up over the lifetime of the star, in units of initial total angular momentum $J_{\text{tot},i}$. These interactions increase in spin up for shorter orbital periods, τ . This is consistent with a characterization of the tidal encounter through a strength parameter η (Press & Teukolsky 1977), for

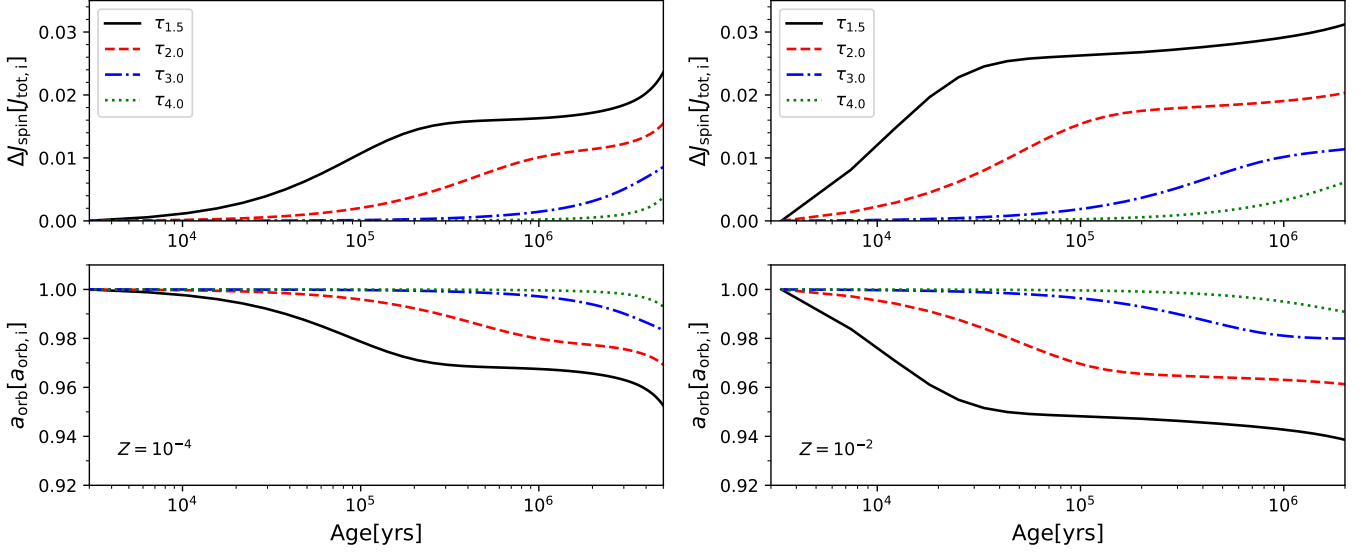


Figure 1. Dependence of massive star spin up on initial orbital period over stellar lifetime, where τ (in the legend) indicates the orbital period in days. In the top row, we show the change in spin angular momentum ΔJ_{spin} , in units of initial total angular momentum $J_{\text{tot},i}$, from an initially non-rotating, massive star of metallicity $Z = 10^{-4}$ (left panel) and $Z = 10^{-2}$ (right panel) from tidal interactions with an orbiting BH companion. In the bottom row, we show the corresponding decrease in orbital separation a_{orb} , in units of initial orbital separation $a_{\text{orb},i}$. These simulations are listed in Table 1 as MS25_BH15_T1.5_Z1.0e-4 to MS25_BH15_T4_Z1.0e-2. The lower metallicity simulations (left panels) show less spin up as the tidal radius (which scales with the stellar radius) is smaller in this case.

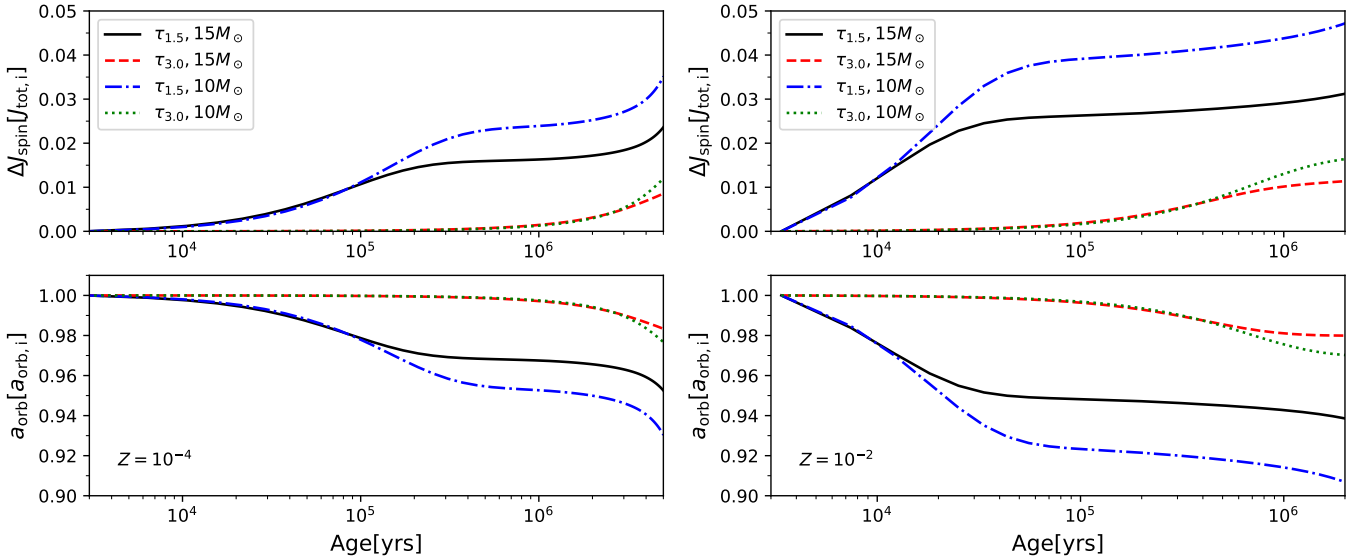


Figure 2. Stellar spin up and orbital separation for the binary at varying mass ratio over stellar lifetime. In the top row, we show the change in spin angular momentum ΔJ_{spin} , in units of initial total angular momentum $J_{\text{tot},i}$, from tidal interactions with an orbiting BH companion. In the bottom row, we show the corresponding decrease in orbital separation a_{orb} , in units of initial orbital separation $a_{\text{orb},i}$. We compare evolution for orbital periods of 1.5 ($\tau_{1.5}$) and 3 days ($\tau_{3.0}$) for fixed stellar mass $M_{\text{MS}} = 25M_{\odot}$ and varying mass ratio $M_{\text{BH}} = 10, 15$ for stellar metallicity $Z = 10^{-4}$ (left panels) and $Z = 10^{-2}$ (right panels). These simulations are listed in Table 1 as MS25_BH15_T1.5_Z1.0e-4, MS25_BH15_T3_Z1.0e-4, MS25_BH10_T1.5_Z1.0e-4, MS25_BH10_T3_Z1.0e-4, MS25_BH15_T1.5_Z1.0e-2, MS25_BH15_T3_Z1.0e-2, MS25_BH10_T1.5_Z1.0e-2, and MS25_BH10_T3_Z1.0e-2.

circular orbits at stellar-BH separation distance a_{orb} ,

$$\eta = \left(\frac{M_*}{M_* + M_{\text{BH}}} \right)^{1/2} \left(\frac{a_{\text{orb}}}{R_*} \right)^{3/2} = \frac{\tau}{\tau_*}, \quad (1)$$

for orbital timescale $\tau = 2\pi\sqrt{a_{\text{orb}}^3/[G(M_* + M_{\text{BH}})]}$ and stellar timescale $\tau_* = 2\pi\sqrt{R_*^3/(GM_*)}$. For a given star, encounters with smaller orbital periods will give rise to smaller η or stronger tidal interactions. For our simulations in Table 1, we consider binaries in the weak or partial disruption regime $\eta > 1$. Note that the limit $\eta = 1$ corresponds to the tidal disruption limit where the dynamical time scales for the orbit and star are comparable. Our tidal calculations relating the spin up of massive star to orbital period for $M_* > M_{\text{BH}}$ using the detailed stellar model described in Sec. 2, agree with results of the spin up of polytropic stars in the weak tidal encounter regime for $M_* < M_{\text{BH}}$ (Kochanek 1992; Khokhlov et al. 1993; Cheng & Evans 2013). Importantly, we find that for a given mass M_* and initial orbital separation $a_{\text{orb},i}$, massive star with lower metallicity (left panel) give rise to lower spin up than higher metallicity (right panel). This decrease in spin is consistent with the encounter strength parameter in Eq. 1, where stars with lower metallicity are more compact and give rise to weaker encounters (larger η) at fixed M_* and orbital separation a_{orb} . In the bottom row, we show the evolution of orbital separation a_{orb} in units of $a_{\text{orb},i}$. For all of these encounters, the massive star is tidally captured, with a decrease in a_{orb} . This is consistent with the orbital separation to tidal radius and mass ratio regime described in the parameter study simulating the interaction between stellar BH and main-sequence stars in Kremer et al. (2022).

The values of the final specific angular momentum of the massive star in cgs units range from $\sim 2 \times 10^{16} \text{cm}^2 \text{s}^{-1}$ to $10^{18} \text{cm}^2 \text{s}^{-1}$. This has important implications for the spin of the BH remnant when this massive star collapses, as well as the angular momentum in the disk that forms around the BH during/just after collapse. We consider this in our Discussion Section below.

3.1.2. Dependence on Mass Ratio

We examine the spin up of the massive star and change in orbital separation over the massive star lifetime for two mass ratios ($M_{\text{MS}}/M_{\text{BH}}$), shown in Fig. 2. For these simulations, we consider orbital periods of 1.5 and 3 days for a $25 M_{\odot}$ massive star with a $10 M_{\odot}$ and $15 M_{\odot}$ BH, at stellar metallicities $Z = 10^{-4}$ and $Z = 10^{-2}$. We find that the more extreme mass ratio encounters (with a $10 M_{\odot}$ BH) lead to a larger spin up. This effect is more pronounced with smaller orbital periods, where

stellar mass loss is greater due to the increase in encounter strength. This is consistent with results shown in de Mink et al. (2013) relating mass and angular momentum loss to mass ratio in interacting binaries.

However, we emphasize that for all of these encounters, the massive star is tidally distorted and there is a decrease in orbital separation a_{orb} of the system, leading to an increase in its spin angular momentum.

3.1.3. Dependence on Initial Spin of the Massive Star

We consider binary encounters where the massive star is initialized over a range of rotational velocities that include non-rotating ($v_0 = 0$), slowly rotating (v_1), and highly rotating ($0.5v_*$) stars. We use $v_1 = 9.177 \times 10^1$ km/s from COSMIC output, as discussed in Kenoly et al. (2023). The break-up velocity v_* is given by $v_* = \{5.199 \times 10^2, 4.450 \times 10^2\}$ km/s for $Z = \{10^{-4}, 10^{-2}\}$, respectively. Fig. 3 shows the stellar spin up and orbital separation at these varying initial rotation velocities, over the massive star lifetime. The evolution of ΔJ_{spin} and a_{orb} are similar for both cases of stellar metallicity. The spin for all three initial rotations reach close to the same value at the end of stellar lifetime. However, we note that when the massive star is initially rapidly rotating ($0.5v_*$), this is the result of the massive star spinning *down* over its lifetime while increasing in orbital separation.

3.2. Stellar Density Profiles

In Figure 4, we show the density profile of the massive star at low and high metallicity ($Z = 10^{-4}$ and $Z = 10^{-2}$, respectively) for the case of an initial orbital period of three days. We expect that when tidal effects are not strong, earlier in the star's life when the binary separation is still relatively large, the low metallicity star is more compact and the stellar density profiles are similar to single massive stars (black lines in Figure 4).

However, when the orbital separation decreases and tidal interactions become important, the companion can have an interesting effect on the density profile of the massive star (which in turn has important implications for the density profile of the circumbinary medium). As we see here, tidal interactions deform the star in such a way that it loses some mass and increases in radius with the likelihood, as discussed in Cheng & Evans (2013), for shock heating in the outer layers.

We expect that tidal interactions with an extended gas around a star may lead to ejection and therefore contribute to the density of the circumbinary environment. Provided that some of this gas settles into the direction into which the GRB jet (that is produced when the massive star collapses) propagates, this can lead to brighter

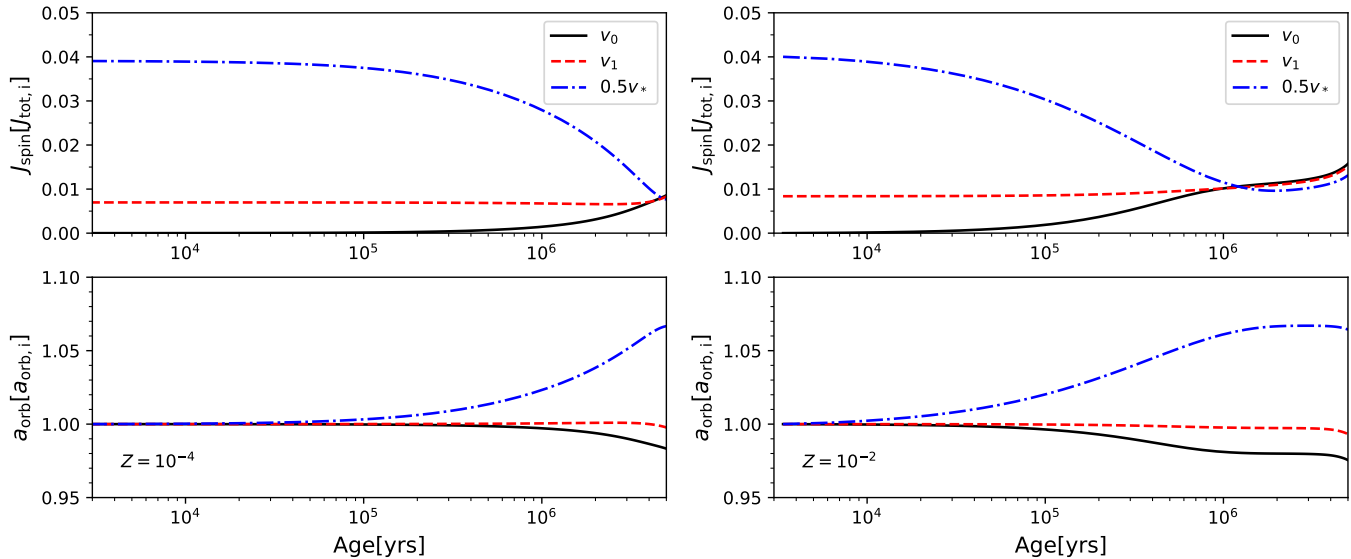


Figure 3. Stellar spin up and orbital separation for the binary at varying initial rotation over stellar lifetime. We consider stellar models identified in Table 1 as MS25_BH15_T3_Z1.0e-4 and MS25_BH15_T3_Z1.0e-2 with an initially non-rotating (v_0), low rotating (v_1), and high rotating ($0.5v_*$) massive star of metallicity $Z = 10^{-4}$ (left panels) and $Z = 10^{-2}$ (right panels). In the top row, we show the change in spin angular momentum ΔJ_{spin} , in units of initial total angular momentum $J_{\text{tot},i}$, from tidal interactions with an orbiting BH companion. In the bottom row, we show the corresponding change in orbital separation a_{orb} , in units of initial orbital separation $a_{\text{orb},i}$. In both cases of stellar metallicity, ΔJ_{spin} and a_{orb} have similar evolution. The spin up for all initial rotations reach close to the same value at the end of stellar evolution. Additionally, the initial velocities of v_0 and v_1 lead to closer orbits while an initial velocity of half the break-up velocity $0.5v_*$ leads to more distant orbits.

radio emission since the radio flux scales as the square root of gas density³ (Sari et al. 1998).

3.3. Additional Tests and Caveats

There are various mechanisms, such as the Spruit-Taylor dynamo, other magnetic coupling effects, or convection effects (Spruit 2002; Heger et al. 2005), that can transport angular momentum out of the star throughout its lifetime. For example, Figure 3 of Heger et al. (2005) shows a pronounced decrease in angular momentum when magnetic fields are present, particularly for the pre-supernova stages of a star’s evolution. However, Denissenkov & Pinsonneault (2007) show that some of the assumptions required to invoke these effects are not always valid and, as a result, the loss of angular momentum can be significantly reduced. Potter et al. (2012) analyze the importance of the Spruit-Taylor dynamo in stars over a range of masses, and find that for stars above about $15M_{\odot}$ it becomes more difficult to sustain the dynamo, and as such the magnetic braking that normally occurs when this dynamo is active may be less severe for more massive stars (particularly in the earlier stages of their evolution). We found that turning this flag on and off did not affect our results. We also investigated the

effects of a rotating convection zone within the massive star. We began this investigation by setting the diffusion coefficients as prescribed in Heger et al. (2000) equal to 0. We find no change in the final angular momentum of the massive star at the end of its lifetime when this flag was turned on.

4. DISCUSSION

We have investigated the properties of a massive star with a closely orbiting compact object companion and find a range of parameter space in which the massive star is spun up (i.e. ends its life with high angular momentum). We conjecture that this then is a plausible model for a highly spinning BH-disk system upon the massive star’s collapse, one that is capable of producing a viable GRB. We note that tidal synchronization is crucial for the massive star to spin up, especially if it begins with low initial angular momentum.

For a tidally locked binary system, the angular momentum of the massive star prior to collapse can be estimated by (Lloyd-Ronning 2022):

$$J_{\text{spin}} \sim M_* R_*^2 \left(\frac{GM_{\text{tot}}}{a_{\text{orb}}^3} \right)^{1/2}, \quad (2)$$

for stellar mass M_* , stellar radius R_* , orbital separation a_{orb} , and where $M_{\text{tot}} = (M_{\text{BH}} + M_*)$ is the total mass of the binary system. The spin up of the massive star

³ This is in the case of optically thin synchrotron emission.

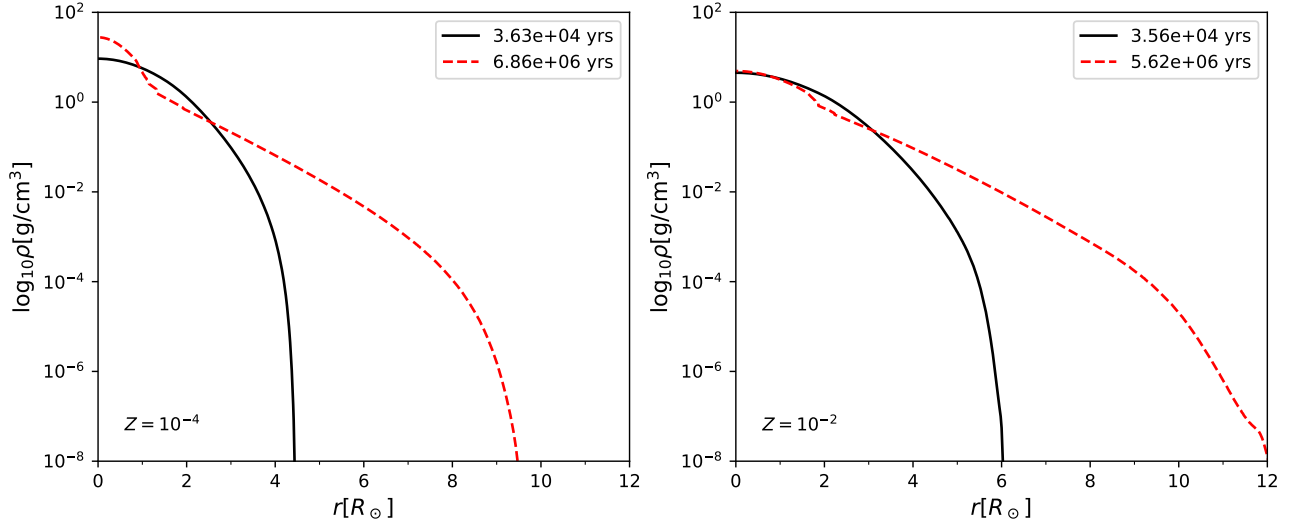


Figure 4. Stellar density profile for a $25 M_{\odot}$ star is presented, comparing low metallicity ($Z = 10^{-4}$) in the left panel and high metallicity ($Z = 10^{-2}$) in the right panel. As expected, at early times, the low metallicity star exhibits greater compactness and a smaller radial extent compared to its high metallicity counterpart. However, over time, tidal effects cause the envelope of the low metallicity star to be pulled and extended to nearly two times its initial radius. Nevertheless, the trend persists, showing that lower metallicity stars maintain a smaller radius compared to those with higher metallicity.

we find in our simulations in this work is consistent with this analytic result.

We note that there is additional loss of orbital angular momentum through gravitational radiation (Peters 1964) for which we have not accounted. However, for the orbital separations we consider (Newtonian gravity regime), this is a negligible effect and does not significantly affect our results over the timescales we are considering (Mapelli 2020; Beradze et al. 2020). Other effects (that we do not consider in this study) such as common envelope evolution and dynamical friction can also change the angular momentum loss timescale, significantly affecting the orbital evolution and, in turn, the final angular momentum of the massive star.

In connecting our progenitor system to a GRB - which results when the highly spinning massive star in our system collapses to a black hole - we have also not accounted for the potential loss of angular momentum upon collapse of the star. Here, we are making the assumption that a highly spinning massive star at the end of its life will produce a highly spinning BH-disk system. This is reasonably justified as shown in Jermyn et al. (2021a), who demonstrate that highly spinning massive stars in the ranges we consider end up with a roughly $10M_{\odot}$ BH remnant, with a spin parameter $a \sim 1$, and with a long-lived disk (all elements necessary to launch a relativistic GRB jet). Qin et al. (2018) use MESA to explore a range of conditions, in systems similar to the ones we consider here, where the spin of the second BH is high. They find that for very closely

orbiting binaries, the spin of the second BH (i.e. the BH produced from the massive star in the systems we consider) is indeed near maximum ($a \sim 1$), particularly for low metallicity systems where mass loss from line driven winds is relatively small.

Therefore, under the reasonable assumption of a highly spinning massive star produces a highly spinning BH-disk system, this central engine with high angular momentum will then produce a longer lasting GRB jet. This, in turn, can manifest observationally as longer lasting GRB prompt emission, consistent with what is observed in the class of radio bright GRBs.

We suggest that in some cases (especially for higher metallicity stars with a “puffier” density profile or for more vigorous tidal interactions), a denser (relative to a single massive star) medium may be formed around the binary system to a larger radius and may potentially lead to a brighter radio afterglow, where the radio flux scales as roughly the square root of the circumbinary density (Sari et al. 1998).

The tidal interaction between the black hole and the massive star is the underlying mechanism of the spin up of our massive star, as well as the extended density profile that deviates from the typical $1/r^2$ profile of a single massive star. We note that Sciarini et al. (2024) have pointed out that tidal prescriptions in binary stellar evolution codes can sometimes either over or underestimate the strength of the tidal torque and so

caution must be taken in over-interpreting results.

5. CONCLUSIONS

We have modeled the evolution of a massive star with a closely orbiting compact object companion. Our study is motivated by the interesting result that radio bright GRBs tend to have a longer prompt gamma-ray burst duration compared to radio dark GRBs. As such, we have explored systems that potentially lead to a massive star with more angular momentum (and therefore a longer lived accretion disk and jet which reflects the duration of the prompt emission). We have also discussed the dependence of the density profile of the massive star on binary interaction and stellar metallicity (which has implications for the density of the circumbinary medium).

Our main conclusions are as follows:

- We find that massive stars with closely orbiting compact object companions are significantly spun up through tidal interactions, and end their life with high angular momentum, conducive to producing a highly spinning BH-disk system that could power a relatively long-lived GRB jet. The specific angular momentum of the star at the end of its life aligns with the expectation of the angular momentum needed for a roughly $10 M_{\odot}$ star to launch a relativistic jet through the Blandford-Znajek process (Blandford & Znajek 1977).
- We find tidal effects leading to significant stellar spin up for orbital periods up to about 4 days, and over a range of mass ratios.
- We find that the tidal spin up is more pronounced for higher metallicity stars for a given binary orbital period, due to the larger radius/extent of the star. However, the spin up is still significantly present in low metallicity systems.
- We find that spin up depends strongly on the initial rotation of the massive star. Unsurprisingly, stars with more initial angular momentum are not spun up for the orbital periods we consider. In these cases, tidal syncing causes the massive star to spin down to synchronize with the orbital period of the system.
- We present two sample density profiles of a massive star at two metallicities, illustrating the

greater extent of the higher metallicity star. We discuss how this not only affects tidal interactions but also potentially impacts the density profile of the medium surrounding the binary.

The results of our work here inform future detailed studies into the physics of gamma-ray bursts. Specifically, we use the angular momentum of the massive star at the end of its life to inform our initial BH and disk angular momentum set-up in upcoming general relativistic magnetohydrodynamic simulations of the GRB jet produced by these systems. We find specific angular momenta of the massive star in our closely orbiting binaries consistent with what others have employed in the literature for their BH-disk simulations (e.g. James et al. 2022).

Our work has defined a range of parameter space for specific binary systems that could be viable GRB progenitors, particularly for the sub-class of radio bright GRBs. Our results can be used to model populations of these systems and estimate their rates (A. Cason et al. in prep), validating whether they align with observed rates of long radio bright GRBs.

ACKNOWLEDGMENTS

We thank the MESA community for helpful conversations and the many resources provided to help run MESA. This work was supported by the U. S. Department of Energy through Los Alamos National Laboratory (LANL). LANL is operated by Triad National Security, LLC, for the National Nuclear Security Administration of U.S. Department of Energy (Contract No. 89233218CNA000001). Research presented was supported by the Laboratory Directed Research and Development program of LANL project number 20230115ER. We acknowledge LANL Institutional Computing HPC Resources under project w23extremex. Additional research presented in this article was supported by the Laboratory Directed Research and Development program of Los Alamos National Laboratory under project number 20210808PRD1. LA-UR-24-22983

DATA AVAILABILITY

The data underlying this article will be shared on reasonable request to the corresponding author.

REFERENCES

- Angulo, C., Arnould, M., Rayet, M., et al. 1999, NuPhA, 656, 3, doi: [10.1016/S0375-9474\(99\)00030-5](https://doi.org/10.1016/S0375-9474(99)00030-5)
- Augustson, K. C., & Mathis, S. 2019, The Astrophysical Journal, 874, 83, doi: [10.3847/1538-4357/ab0b3d](https://doi.org/10.3847/1538-4357/ab0b3d)

- Barkov, M. V., & Komissarov, S. S. 2008, *International Journal of Modern Physics D*, 17, 1669, doi: [10.1142/S0218271808013285](https://doi.org/10.1142/S0218271808013285)
- Beradze, R., Gogberashvili, M., & Sakharov, A. S. 2020, *Physics Letters B*, 804, 135402, doi: [10.1016/j.physletb.2020.135402](https://doi.org/10.1016/j.physletb.2020.135402)
- Blandford, R. D., & Znajek, R. L. 1977, *MNRAS*, 179, 433, doi: [10.1093/mnras/179.3.433](https://doi.org/10.1093/mnras/179.3.433)
- Bloom, J. S., Kulkarni, S. R., & Djorgovski, S. G. 2002, *AJ*, 123, 1111, doi: [10.1086/338893](https://doi.org/10.1086/338893)
- Blouin, S., Shaffer, N. R., Saumon, D., & Starrett, C. E. 2020, *ApJ*, 899, 46, doi: [10.3847/1538-4357/ab9e75](https://doi.org/10.3847/1538-4357/ab9e75)
- Breivik, K., Coughlin, S., Zevin, M., et al. 2020, *ApJ*, 898, 71, doi: [10.3847/1538-4357/ab9d85](https://doi.org/10.3847/1538-4357/ab9d85)
- Cassisi, S., Potekhin, A. Y., Pietrinferni, A., Catelan, M., & Salaris, M. 2007, *ApJ*, 661, 1094, doi: [10.1086/516819](https://doi.org/10.1086/516819)
- Cehula, J., & Pejcha, O. 2023, *MNRAS*, 524, 471, doi: [10.1093/mnras/stad1862](https://doi.org/10.1093/mnras/stad1862)
- Chakraborty, A., Dainotti, M., Cantrell, O., & Lloyd-Ronning, N. 2023, *MNRAS*, 520, 5764, doi: [10.1093/mnras/stad438](https://doi.org/10.1093/mnras/stad438)
- Cheng, R. M., & Evans, C. R. 2013, *PhRvD*, 87, 104010, doi: [10.1103/PhysRevD.87.104010](https://doi.org/10.1103/PhysRevD.87.104010)
- Chugunov, A. I., Dewitt, H. E., & Yakovlev, D. G. 2007, *PhRvD*, 76, 025028, doi: [10.1103/PhysRevD.76.025028](https://doi.org/10.1103/PhysRevD.76.025028)
- Cyburt, R. H., Amthor, A. M., Ferguson, R., et al. 2010, *ApJS*, 189, 240, doi: [10.1088/0067-0049/189/1/240](https://doi.org/10.1088/0067-0049/189/1/240)
- de Mink, S. E., Langer, N., Izzard, R. G., Sana, H., & de Koter, A. 2013, *ApJ*, 764, 166, doi: [10.1088/0004-637X/764/2/166](https://doi.org/10.1088/0004-637X/764/2/166)
- Denissenkov, P. A., & Pinsonneault, M. 2007, *ApJ*, 655, 1157, doi: [10.1086/510345](https://doi.org/10.1086/510345)
- Eggleton, P. P. 1983, *ApJ*, 268, 368, doi: [10.1086/160960](https://doi.org/10.1086/160960)
- Falanga, M., Bozzo, E., Lutovinov, A., et al. 2015, *A&A*, 577, A130, doi: [10.1051/0004-6361/201425191](https://doi.org/10.1051/0004-6361/201425191)
- Ferguson, J. W., Alexander, D. R., Allard, F., et al. 2005, *ApJ*, 623, 585, doi: [10.1086/428642](https://doi.org/10.1086/428642)
- Fruchter, A. S., Thorsett, S. E., Metzger, M. R., et al. 1999, *ApJL*, 519, L13, doi: [10.1086/312094](https://doi.org/10.1086/312094)
- Fruchter, A. S., Levan, A. J., Strolger, L., et al. 2006, *Nature*, 441, 463, doi: [10.1038/nature04787](https://doi.org/10.1038/nature04787)
- Fuller, G. M., Fowler, W. A., & Newman, M. J. 1985, *ApJ*, 293, 1, doi: [10.1086/163208](https://doi.org/10.1086/163208)
- Graham, J. F., & Fruchter, A. S. 2013, *ApJ*, 774, 119, doi: [10.1088/0004-637X/774/2/119](https://doi.org/10.1088/0004-637X/774/2/119)
- . 2017, *ApJ*, 834, 170, doi: [10.3847/1538-4357/834/2/170](https://doi.org/10.3847/1538-4357/834/2/170)
- Graham, J. F., Schady, P., & Fruchter, A. S. 2019, arXiv e-prints. <https://arxiv.org/abs/1904.02673>
- Heger, A., Langer, N., & Woosley, S. E. 2000, *The Astrophysical Journal*, 528, 368, doi: [10.1086/308158](https://doi.org/10.1086/308158)
- Heger, A., Woosley, S. E., & Spruit, H. C. 2005, *ApJ*, 626, 350, doi: [10.1086/429868](https://doi.org/10.1086/429868)
- Hirschi, R., Meynet, G., & Maeder, A. 2005, *A&A*, 443, 581, doi: [10.1051/0004-6361:20053329](https://doi.org/10.1051/0004-6361:20053329)
- Hjorth, J., & Bloom, J. S. 2012, *Gamma-ray bursts*
- Hjorth, J., Sollerman, J., Møller, P., et al. 2003, *Nature*, 423, 847, doi: [10.1038/nature01750](https://doi.org/10.1038/nature01750)
- Hurley, J. R., Pols, O. R., & Tout, C. A. 2000, *MNRAS*, 315, 543, doi: [10.1046/j.1365-8711.2000.03426.x](https://doi.org/10.1046/j.1365-8711.2000.03426.x)
- Hurley, J. R., Tout, C. A., & Pols, O. R. 2002, *MNRAS*, 329, 897, doi: [10.1046/j.1365-8711.2002.05038.x](https://doi.org/10.1046/j.1365-8711.2002.05038.x)
- Iglesias, C. A., & Rogers, F. J. 1993, *ApJ*, 412, 752, doi: [10.1086/172958](https://doi.org/10.1086/172958)
- . 1996, *ApJ*, 464, 943, doi: [10.1086/177381](https://doi.org/10.1086/177381)
- Irwin, A. W. 2004, *The FreeEOS Code for Calculating the Equation of State for Stellar Interiors*. <http://freeeos.sourceforge.net/>
- Itoh, N., Hayashi, H., Nishikawa, A., & Kohyama, Y. 1996, *ApJS*, 102, 411, doi: [10.1086/192264](https://doi.org/10.1086/192264)
- James, B., Janiuk, A., & Nouri, F. H. 2022, *ApJ*, 935, 176, doi: [10.3847/1538-4357/ac81b7](https://doi.org/10.3847/1538-4357/ac81b7)
- Jermyn, A. S., Dittmann, A. J., Cantiello, M., & Perna, R. 2021a, *ApJ*, 914, 105, doi: [10.3847/1538-4357/abfb67](https://doi.org/10.3847/1538-4357/abfb67)
- Jermyn, A. S., Schwab, J., Bauer, E., Timmes, F. X., & Potekhin, A. Y. 2021b, *ApJ*, 913, 72, doi: [10.3847/1538-4357/abf48e](https://doi.org/10.3847/1538-4357/abf48e)
- Jermyn, A. S., Bauer, E. B., Schwab, J., et al. 2023, *ApJS*, 265, 15, doi: [10.3847/1538-4365/aca8d](https://doi.org/10.3847/1538-4365/aca8d)
- Kelley, R. L., Rappaport, S., Clark, G. W., & Petro, L. D. 1983, *ApJ*, 268, 790, doi: [10.1086/161001](https://doi.org/10.1086/161001)
- Kenoly, L., Luu, A. K., Toral, C., et al. 2023, *Research Notes of the American Astronomical Society*, 7, 167, doi: [10.3847/2515-5172/aced00](https://doi.org/10.3847/2515-5172/aced00)
- Khokhlov, A., Novikov, I. D., & Pethick, C. J. 1993, *ApJ*, 418, 163, doi: [10.1086/173379](https://doi.org/10.1086/173379)
- King, A. R., & Pringle, J. E. 2021, arXiv e-prints, arXiv:2107.12384. <https://arxiv.org/abs/2107.12384>
- Kochanek, C. S. 1992, *ApJ*, 385, 604, doi: [10.1086/170966](https://doi.org/10.1086/170966)
- Kolb, U., & Ritter, H. 1990, *A&A*, 236, 385
- Komissarov, S. S., & Barkov, M. V. 2009, *MNRAS*, 397, 1153, doi: [10.1111/j.1365-2966.2009.14831.x](https://doi.org/10.1111/j.1365-2966.2009.14831.x)
- Kremer, K., Lombardi, J. C., Lu, W., Piro, A. L., & Rasio, F. A. 2022, *The Astrophysical Journal*, 933, 203, doi: [10.3847/1538-4357/ac714f](https://doi.org/10.3847/1538-4357/ac714f)
- Kumar, P., Narayan, R., & Johnson, J. L. 2008a, *Science*, 321, 376, doi: [10.1126/science.1159003](https://doi.org/10.1126/science.1159003)
- . 2008b, *MNRAS*, 388, 1729, doi: [10.1111/j.1365-2966.2008.13493.x](https://doi.org/10.1111/j.1365-2966.2008.13493.x)
- Langanke, K., & Martínez-Pinedo, G. 2000, *Nuclear Physics A*, 673, 481, doi: [10.1016/S0375-9474\(00\)00131-7](https://doi.org/10.1016/S0375-9474(00)00131-7)

- Le Floch, E., Duc, P.-A., Mirabel, I. F., et al. 2003, *A&A*, 400, 499, doi: [10.1051/0004-6361:20030001](https://doi.org/10.1051/0004-6361:20030001)
- Levesque, E. M., Kewley, L. J., Graham, J. F., & Fruchter, A. S. 2010, *ApJL*, 712, L26, doi: [10.1088/2041-8205/712/1/L26](https://doi.org/10.1088/2041-8205/712/1/L26)
- Levine, A., Rappaport, S., Deeter, J. E., Boynton, P. E., & Nagase, F. 1993, *ApJ*, 410, 328, doi: [10.1086/172750](https://doi.org/10.1086/172750)
- Levine, A. M., Rappaport, S. A., & Zojcheski, G. 2000, *ApJ*, 541, 194, doi: [10.1086/309398](https://doi.org/10.1086/309398)
- Lloyd-Ronning, N. 2022, *ApJ*, 928, 104, doi: [10.3847/1538-4357/ac54b3](https://doi.org/10.3847/1538-4357/ac54b3)
- Lloyd-Ronning, N. M., Fryer, C., Miller, J. M., et al. 2019a, *MNRAS*, 485, 203, doi: [10.1093/mnras/stz390](https://doi.org/10.1093/mnras/stz390)
- Lloyd-Ronning, N. M., & Fryer, C. L. 2017, *MNRAS*, 467, 3413, doi: [10.1093/mnras/stx313](https://doi.org/10.1093/mnras/stx313)
- Lloyd-Ronning, N. M., Gompertz, B., Pe'er, A., Dainotti, M., & Fruchter, A. 2019b, *ApJ*, 871, 118, doi: [10.3847/1538-4357/aaf6ac](https://doi.org/10.3847/1538-4357/aaf6ac)
- Lyman, J. D., Levan, A. J., Tanvir, N. R., et al. 2017, *MNRAS*, 467, 1795, doi: [10.1093/mnras/stx220](https://doi.org/10.1093/mnras/stx220)
- MacFadyen, A. I., & Woosley, S. E. 1999, *ApJ*, 524, 262, doi: [10.1086/307790](https://doi.org/10.1086/307790)
- Mapelli, M. 2020, *Frontiers in Astronomy and Space Sciences*, 7, 38, doi: [10.3389/fspas.2020.00038](https://doi.org/10.3389/fspas.2020.00038)
- Marchant, P. 2019, *Stellar rotation in binary systems*, 9793, Zenodo, doi: [10.5281/zenodo.5565258](https://doi.org/10.5281/zenodo.5565258)
- Mink, S. D. 2019, *Massive binaries*, 9793, Zenodo, doi: [10.5281/zenodo.2603594](https://doi.org/10.5281/zenodo.2603594)
- Oda, T., Hino, M., Muto, K., Takahara, M., & Sato, K. 1994, *Atomic Data and Nuclear Data Tables*, 56, 231, doi: [10.1006/adnd.1994.1007](https://doi.org/10.1006/adnd.1994.1007)
- Palla, M., Matteucci, F., Calura, F., & Longo, F. 2019, arXiv e-prints. <https://arxiv.org/abs/1903.01353>
- Paxton, B. 2021, *Modules for Experiments in Stellar Astrophysics (MESA)*, r21.12.1, Zenodo, doi: [10.5281/zenodo.5798242](https://doi.org/10.5281/zenodo.5798242)
- Paxton, B., Bildsten, L., Dotter, A., et al. 2011, *ApJS*, 192, 3, doi: [10.1088/0067-0049/192/1/3](https://doi.org/10.1088/0067-0049/192/1/3)
- Paxton, B., Cantiello, M., Arras, P., et al. 2013, *ApJS*, 208, 4, doi: [10.1088/0067-0049/208/1/4](https://doi.org/10.1088/0067-0049/208/1/4)
- Paxton, B., Marchant, P., Schwab, J., et al. 2015, *ApJS*, 220, 15, doi: [10.1088/0067-0049/220/1/15](https://doi.org/10.1088/0067-0049/220/1/15)
- Paxton, B., Schwab, J., Bauer, E. B., et al. 2018, *ApJS*, 234, 34, doi: [10.3847/1538-4365/aaa5a8](https://doi.org/10.3847/1538-4365/aaa5a8)
- Paxton, B., Smolec, R., Schwab, J., et al. 2019, *ApJS*, 243, 10, doi: [10.3847/1538-4365/ab2241](https://doi.org/10.3847/1538-4365/ab2241)
- Peters, P. C. 1964, *Physical Review*, 136, 1224, doi: [10.1103/PhysRev.136.B1224](https://doi.org/10.1103/PhysRev.136.B1224)
- Potekhin, A. Y., & Chabrier, G. 2010, *Contributions to Plasma Physics*, 50, 82, doi: [10.1002/ctpp.201010017](https://doi.org/10.1002/ctpp.201010017)
- Potter, A. T., Chitre, S. M., & Tout, C. A. 2012, *MNRAS*, 424, 2358, doi: [10.1111/j.1365-2966.2012.21409.x](https://doi.org/10.1111/j.1365-2966.2012.21409.x)
- Poutanen, J. 2017, *ApJ*, 835, 119, doi: [10.3847/1538-4357/835/2/119](https://doi.org/10.3847/1538-4357/835/2/119)
- Press, W. H., & Teukolsky, S. A. 1977, *ApJ*, 213, 183, doi: [10.1086/155143](https://doi.org/10.1086/155143)
- Qin, Y., Fragos, T., Meynet, G., et al. 2018, *A&A*, 616, A28, doi: [10.1051/0004-6361/201832839](https://doi.org/10.1051/0004-6361/201832839)
- Ritter, H. 1988, *A&A*, 202, 93
- Rogers, F. J., & Nayfonov, A. 2002, *ApJ*, 576, 1064, doi: [10.1086/341894](https://doi.org/10.1086/341894)
- Sari, R., Piran, T., & Narayan, R. 1998, *ApJL*, 497, L17, doi: [10.1086/311269](https://doi.org/10.1086/311269)
- Saumon, D., Chabrier, G., & van Horn, H. M. 1995, *ApJS*, 99, 713, doi: [10.1086/192204](https://doi.org/10.1086/192204)
- Sciarini, L., Ekström, S., Eggenberger, P., et al. 2024, *A&A*, 681, L1, doi: [10.1051/0004-6361/202348424](https://doi.org/10.1051/0004-6361/202348424)
- Spruit, H. C. 2002, *A&A*, 381, 923, doi: [10.1051/0004-6361:20011465](https://doi.org/10.1051/0004-6361:20011465)
- Tauris, T. M., & van den Heuvel, E. P. J. 2006, in *Compact stellar X-ray sources*, Vol. 39, 623–665
- Timmes, F. X., & Swesty, F. D. 2000, *ApJS*, 126, 501, doi: [10.1086/313304](https://doi.org/10.1086/313304)
- Woosley, S., & Bloom, J. 2006, *Annu. Rev. Astron. Astrophys.*, 44, 507
- Woosley, S. E. 1993, *ApJ*, 405, 273, doi: [10.1086/172359](https://doi.org/10.1086/172359)
- Woosley, S. E., & Heger, A. 2006, *ApJ*, 637, 914, doi: [10.1086/498500](https://doi.org/10.1086/498500)
- Yoon, S.-C., & Langer, N. 2005, *A&A*, 443, 643, doi: [10.1051/0004-6361:20054030](https://doi.org/10.1051/0004-6361:20054030)
- Yoon, S.-C., Langer, N., & Norman, C. 2006, *A&A*, 460, 199, doi: [10.1051/0004-6361:20065912](https://doi.org/10.1051/0004-6361:20065912)

6. APPENDIX

6.1. *Convergence study of MESA simulations*

We have simulated the change of orbital parameters over the lifetime of the massive star, prior to collapse, tracking the evolution of quantities such as orbital separation of the binary a_{orb} , mass of the star M_* , and change in spin, orbital, and total angular momentum ΔJ as well as stellar profiles such as density and pressure. We consider numerical convergence where these quantities do not change appreciably over stellar lifetime at increasing mass resolution. In Fig. 5, we show consistent evolution over stellar age, in years, in stellar spin up ΔJ_{spin} , normalized by the initial total angular momentum $\Delta J_{\text{tot},i}$, and orbital separation a_{orb} , normalized by the initial orbital separation $a_{\text{orb},i}$ as well as evolution of carbon-oxygen core mass $M_{\text{CO, core}}$ and stellar central temperature T for binary models MS25_BH15_T3.0_Z1.0e-4 (left panel) and MS25_BH15_T3.0_Z1.0e-2 (right panel) for fixed mass ratio and initial orbital period at increasing mass resolution set in MESA by *max_dq* at 1.0e-2 (Δ_0), 1.0e-3 (Δ_1), and 1.0e-4 (Δ_2). We find similar trends for both choices in metallicity $Z = 10^{-2}$ and $Z = 10^{-4}$. In Fig. 6, we consider the evolution in model number of stellar spin up and orbital separation for the binary at increasing mass resolution using the models given in Fig. 5. We show comparably smooth changes for each resolution in stellar age, given in years, for the evolution of binary parameters. For all other simulation results, we use the highest mass resolution, Δ_2 .

6.2. *End point in MESA simulations of interacting binaries*

We report the maximum spin up of the massive star due to the tidal interaction with the orbiting black hole prior to collapse. Our simulations capture the angular momentum transfer in a binary treatment within the one-dimensional stellar evolution MESA code. We consider the end point in our simulations as prior to collapse, when the carbon-oxygen core forms. At this stage in the evolution, a full multi-dimensional treatment of the interaction is necessary to capture the asymmetrical, hydrodynamic response of the star to the orbiting black hole. For all of the models given in Table 1, as in Fig. 5, we identify a maximum peak value for the spin angular momentum that occurs just prior the rapid increase in mass of the carbon-oxygen core.

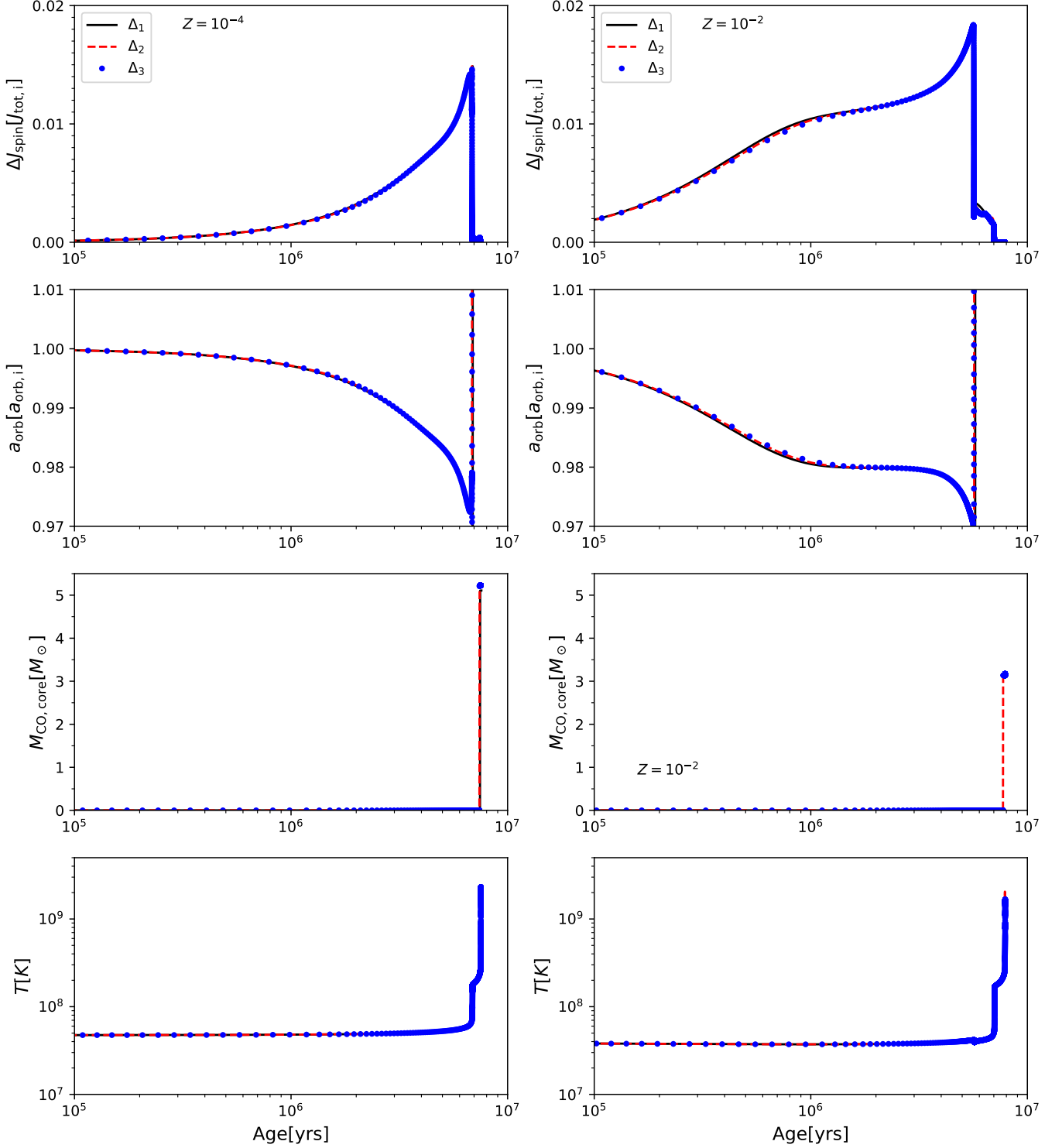


Figure 5. Numerical convergence of stellar spin up and orbital separation for the binary at increasing mass resolution. We compare simulation results of models MS25_BH15_T3.0_Z1.0e-4 and MS25_BH15_T3.0_Z1.0e-2 for fixed mass ratio and initial orbital period at three levels of resolution set in *MESA* at 1.0e-2 (Δ_0), 1.0e-3 (Δ_1), and 1.0e-4 (Δ_2). In stellar age, given in years, we show convergence in the evolution of the binary parameters of change in spin angular momentum ΔJ_{spin} , in units of initial total angular momentum $J_{\text{tot},i}$ and orbital separation a_{orb} , in units of initial orbital separation $a_{\text{orb},i}$, as well as stellar parameters of carbon-oxygen core mass $M_{\text{CO, core}}$ and central temperature T in stellar metallicity $Z = 10^{-4}, 10^{-2}$ (left and right panels, respectively).

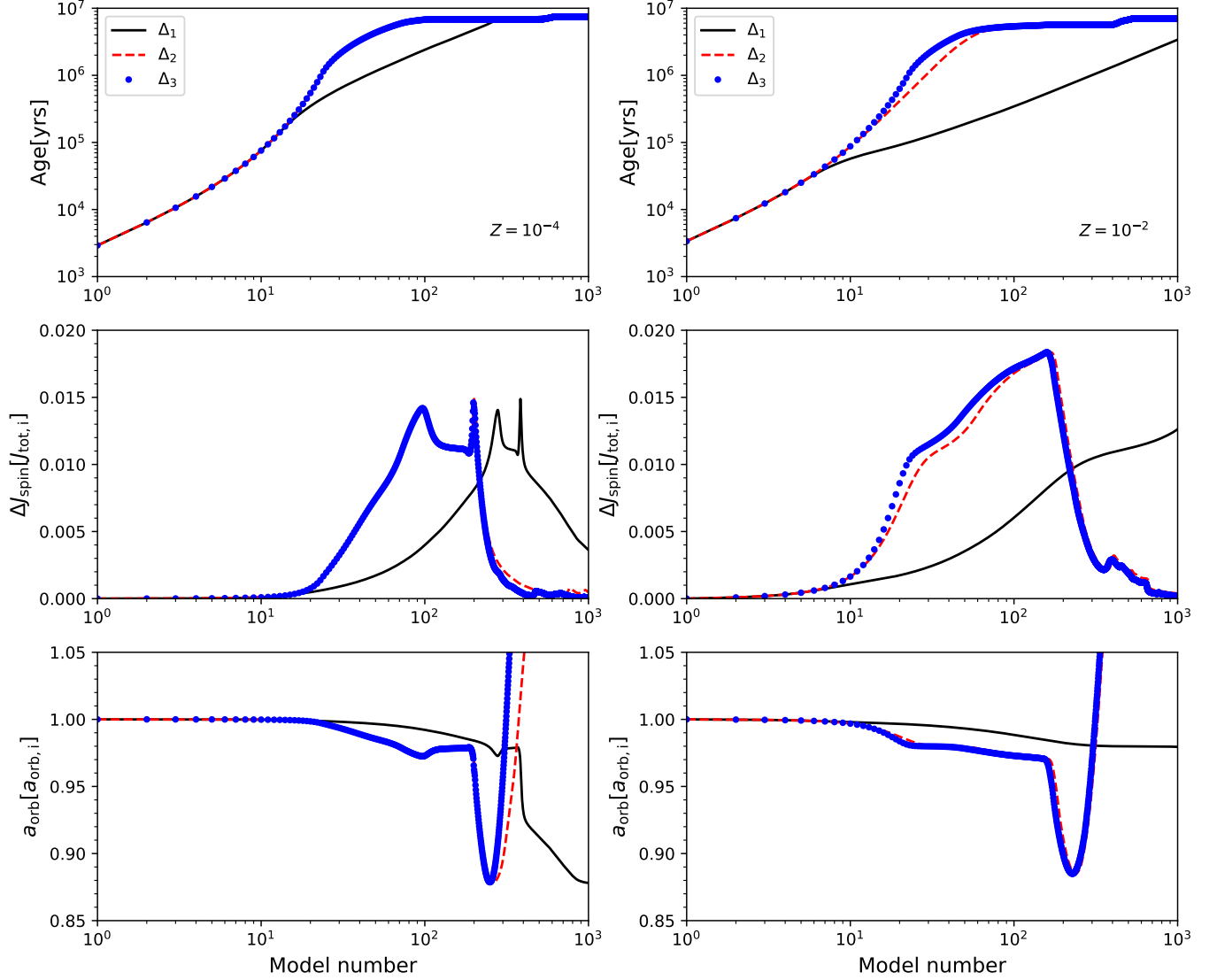


Figure 6. Evolution in model number of stellar spin up and orbital separation for the binary at increasing mass resolution. We compare simulation results of models MS25_BH15_T3.0_Z1.0e-4 and MS25_BH15_T3.0_Z1.0e-2 for fixed mass ratio and initial orbital period at three levels of resolution set in MESA

at $1.0e-2$ (Δ_0), $1.0e-3$ (Δ_1), and $1.0e-4$ (Δ_2). In model number, we show comparably smooth changes for each resolution in stellar age, given in years, and the evolution of the binary parameters of change in spin angular momentum ΔJ_{spin} , in units of initial total angular momentum $J_{\text{tot},i}$ and orbital separation a_{orb} , in units of initial orbital separation $a_{\text{orb},i}$, in stellar metallicity $Z = 10^{-4}, 10^{-2}$ (left and right panels, respectively).